Multielectron Correlation in High-Harmonic Generation: A 2D Model Analysis

Suren Sukiasyan,[1,2,*] Chris McDonald,[1] Carlos Destefani,[1] Misha Yu. Ivanov,[2] and Thomas Brabec[1]

[1]*Physics Department and Center for Research in Photonics, University of Ottawa, 150 Louis Pasteur, Ottawa, Ontario K1N 6N5, Canada*

[2]*National Research Council, 100 Sussex Drive, Ottawa, Ontario K1A 0R6, Canada*

(Received 21 December 2007; revised manuscript received 31 October 2008; published 5 June 2009)

We analyze the role of multielectron dynamics in high-harmonic generation spectroscopy, using an example of a two-electron system. We identify and systematically quantify the importance of correlation and exchange effects. One of the main sources for correlation is identified to be the polarization of the ion by the recombining continuum electron. This effect, which plays an important qualitative and quantitative role, seriously undermines the validity of the standard approaches to high-harmonic generation, which ignore the contribution of excited ionic states to the radiative recombination of the continuum electron.

DOI: 10.1103/PhysRevLett.102.223002 PACS numbers: 32.80.Rm, 32.80.Wr

High-harmonic generation (HHG) takes place when a gas of atoms or molecules is exposed to an intense laser pulse, yielding harmonics of the incident field with orders up to several hundreds [1]. In addition to being the workhorse for modern attosecond pulse technology [2], HHG offers the potential for resolving fundamental microscopic processes with sub-Å spatial and subfemtosecond temporal resolution [3–5].

Applications of HHG to attosecond dynamic imaging and molecular tomography typically rely on the three-step model [6]. An electron is (i) liberated from the highest occupied orbital, (ii) accelerated by the intense laser field, and (iii) emits a harmonic photon upon returning to the parent ion and recombining to the initial bound state of the neutral. This model uses the single active electron (SAE) approximation, with only the weakest bound electron interacting with the laser field.

The importance and the exact role of multielectron effects in HHG remain unclear. Already in the frozen-core approximation, multielectron effects are indispensable for the tomographic retrieval of wave functions [7–9]. It is clear that exchange and correlation should play a role in HHG [10]. However, little is known about the specific ways in which correlation effects manifest themselves. This lack of qualitative and quantitative understanding is a serious bottleneck for applications of HHG to attosecond dynamic imaging [3–5].

This bottleneck exists decades after the discovery of HHG due to fundamental difficulties in the analysis of intense field multielectron dynamics. First, solution of the time-dependent multielectron Schrödinger equation is beyond reach [11–13]. Approximate methods, such as the time-dependent Hartree-Fock (TD HF) [14], frozen-core (fc) [15], and time-dependent density functional theory [16] neglect all or a part of the electron correlation; their accuracy is not controlled. Second, even if the Schrödinger equation is solved, extracting the underlying physical mechanisms from the multidimensional wave function is a formidable problem in its own right.

We report progress on both challenges. We solve the time-dependent Schrödinger equation for HHG in a two-electron model diatomic molecule with two spatial dimensions per electron. Our numerical analysis builds on the multiconfiguration time-dependent Hartree (MCTDH) method [17]. Together with the multiconfiguration time-dependent Hartree-Fock (MCTDHF) method, pioneered in strong-field dynamics in [18,19], it provides consistent *ab initio* framework for tracking multielectron effects. Our optimization of the multiconfiguration expansion brings the computational costs of a converged two-electron calculation down to a level comparable with conventional one-electron calculations and opens the door to a systematic analysis of multielectron effects in HHG. As for the second challenge, we develop an approach that allows us to systematically identify and quantify the physical mechanisms underlying multielectron effects in HHG.

Multielectron effects arise from (i) electron exchange, (ii) polarization and excitation of the neutral and the ion by the laser field, and (iii) polarization and excitation of the ion by the recolliding electron. While the second effect has been considered by [18], the last has been mostly disregarded. We show that the interplay between the recolliding electron and the ion is essential for quantitative modeling of HHG. It may not only enhance [10], but also suppress HHG, depending on the constructive or destructive interference of the harmonic signals generated via channels associated with different ionic states.

Our analysis uses the MCTDH approach [17]. For two electrons in 2D each, we expand the full 4D wave function in sums over products of lower dimensional orbitals. In contrast to the conventional Hartree or HF methods, an MCTDH orbital is a mathematical object that does not necessarily represent a single particle. The choice of the orbitals crucially influences the efficiency of MCTDH. We

have chosen the expansion orbitals to be 1D functions, $\varphi_j(x,t)$, yielding

$$\Psi(x_1,y_1;x_2,y_2,t)=\sum_{j_1=1}^{n_1}\cdots\sum_{j_4=1}^{n_4}A_{j_1j_2j_3j_4}(t)\varphi_{j_1}(x_1,t)\times\varphi_{j_2}(y_1,t)\varphi_{j_3}(x_2,t)\varphi_{j_4}(y_2,t) \quad (1)$$

for the 4D wave function Ψ. Here, $A_{j_1j_2j_3j_4}(t)$ are the expansion coefficients, and n_1, n_2, n_3, n_4 represent the number of expansion functions along the coordinates $\mathbf{r}_1=(x_1,y_1)$ and $\mathbf{r}_2=(x_2,y_2)$, respectively.

The equations of motion for $A(t)$ and $\varphi_j(x,t)$ are derived from the variational principle, see, e.g., [17] (Sec. 3.1). For our Hamiltonian, the initial spin state is conserved and can be factored out. By comparison, in MCTDHF [18,19], the spin is the part of the expansion orbitals and remains in the calculation. We start with the singlet state, for which the spatial part of the wave function Ψ is symmetric. This symmetry is preserved during propagation. The initial (ground) state is calculated by imaginary time propagation [17] (Sec. 7.1).

Our model system uses soft-core Coulomb potentials for both nuclear-electron and electron-electron interactions, $V(x,y)\propto(x^2+y^2+a^2)^{-1/2}$. The soft-core parameter $a=0.64$ is chosen to reproduce the N_2 ionization potential of 15.8 eV and the two-electron binding energy of 46.8 eV. Two nuclei ($Z=1$) are held fixed at the N_2 equilibrium internuclear distance of $R=2.08$ a.u.. The laser field is linearly polarized, $E(t)=E_0\sin^2(\pi t/T)\cos(\omega t)$, with a peak intensity of 10^{14} W/cm^2, a wavelength of 800 nm, and a pulse duration $T=10T_0$, where $T_0=2\pi/\omega=2.6$ fs. Angle θ between the field polarization and the nuclear axis is fixed. The calculation is performed in the length gauge. A grid spacing of 0.4 a.u. is sufficient.

One of the critical issues is calculating the matrix elements of the electron-electron interaction. The expansion

$$V_{ee}(x_1,y_1;x_2,y_2)=\frac{1}{\sqrt{(x_1-x_2)^2+(y_1-y_2)^2+a^2}}=\sum_i v_i(x_1-x_2)u_i(y_1-y_2) \quad (2)$$

in the basis of natural potentials v_i and u_i [17] (Secs. 6.1, 6.2), yields matrix elements of the type $\langle\varphi_{j_1}(x_1)\varphi_{j_2}(x_2)\mid v_i(x_1-x_2)\mid\varphi_{l_1}(x_1)\varphi_{l_2}(x_2)\rangle$. Using the convolution theorem combined with the fast Fourier transform results in a nearly linear scaling with the number of grid points.

We use an absorbing potential of the form $W(x)=-i\eta(|x|-x_c)^3$ in each coordinate for $|x|\geq x_c$, with $\eta=0.0005$. For our laser parameters, we use $x_c=16$ a.u. to absorb the so-called "long" trajectories while keeping the short trajectories, which dominate experimental harmonic spectra [1], intact. This approximation has no influence on the multielectron physics under study. Convergence of the calculation with respect to the number of configurations is determined by diagonalizing the reduced density matrix [17] (Sec. 3.3). Its eigenvalues are the populations of the so-called natural orbitals (the eigenstates of the reduced density matrix.) For $n_1=n_2=n_3=n_4=15$ the lowest eigenvalue remains below 10^{-6} at all times. A HHG calculation takes below 4 h on a single core Intel 3.0 GHz CPU.

To analyze the role of the multielectron dynamics in HHG, we introduce the method of ionic eigenstate-resolved (IER) wave functions. Theses wave functions are determined by projecting the exact wave function $\Psi(\mathbf{r}_1,\mathbf{r}_2,t)$ onto the complete set of the ionic eigenstates, $\psi_k(\mathbf{r}_2)$, i.e., $\phi_k(\mathbf{r}_1,t)=\langle\psi_k(\mathbf{r}_2)\mid\Psi(\mathbf{r}_1,\mathbf{r}_2,t)\rangle$. After symmetrization with respect to the electrons we obtain

$$\Psi_M(\mathbf{r}_1,\mathbf{r}_2,t)=\sum_{k=1}^{M}[\phi_k(\mathbf{r}_1,t)\psi_k(\mathbf{r}_2)+\psi_k(\mathbf{r}_1)\phi_k(\mathbf{r}_2,t)] \quad (3)$$

with M the number of ionic eigenstates. The binding energies of the first four ionic eigenstates are -31 eV, -20.4 eV, -15 eV, and -10.9 eV, respectively. As the ionic eigenfunctions ψ_j are contained in ϕ_k, symmetrization leads to an overcomplete basis; i.e., the terms $\langle\psi_j|\phi_k\rangle\psi_k\psi_j$ with $j=1,\ldots,M$ are counted twice. This can be remedied by substituting $\phi_k\rightarrow(1-\hat{P})\phi_k$ in (3). The projector $\hat{P}=(1/2)\sum_{j=1}^{M}\mid\psi_j(\mathbf{r})\rangle\langle\psi_j(\mathbf{r})\mid$ removes the double counted contributions.

Harmonic spectra are calculated in the acceleration gauge as

$$I_M(\Omega)=4\left|\int\langle\Psi_M|\frac{\partial V}{\partial x_1}+E(t)|\Psi_M\rangle e^{i\Omega t}dt\right|^2. \quad (4)$$

For a systematic analysis of different approximations, we also use

$$I_M^G(\Omega)=4\left|\int\langle\alpha(t)\Psi_g|\frac{\partial V}{\partial x_1}+E(t)|\Psi_M\rangle e^{i\Omega t}dt\right|^2. \quad (5)$$

Here, $\alpha(t)=\langle\Psi_g\mid\Psi(t)\rangle$, Ψ_g is the two-electron ground state, V is the potential of the nuclei, $E(t)$ is the laser electric field, and the factor 4 arises from the electron exchange symmetry. Our analysis is restricted to emission along the laser polarization (x axis). The ansatz Ψ_M describes well the part of the wave function with one electron bound and one in the continuum. Thus, it is best suited for analyzing harmonics with energies above the ionization potential I_p, i.e., beyond the 11th harmonic order in our case. Replacing Ψ_M with Ψ in Eqs. (4) and (5) yields the converged full spectra, I and I^G, respectively.

Inserting Eq. (3) into the Schrödinger equation and multiplying with $\langle\psi_j\mid$ on the left side yields

$$i\partial_t\phi_j(\mathbf{r}_1,t)+i\sum_k\langle\psi_j\mid\partial_t\phi_k(t)\rangle\psi_k(\mathbf{r}_1)=\sum_k\langle\psi_j\mid\mathbf{H}\mid\psi_k\rangle\phi_k(\mathbf{r}_1,t)+\langle\psi_j\mid\mathbf{H}\mid\phi_k(t)\rangle\psi_k(\mathbf{r}_1). \quad (6)$$

Here $\mathbf{H}$ is the total two-electron Hamiltonian and the bracket denotes integration over $\mathbf{r}_2$. Equation (6) shows how to extract information on the multielectron effects by looking at the role of different ionic eigenstates. For $M = 1$, Eq. (3) describes the part of the exact wave function, where one electron remains in the ionic ground state. It is the closest possible to the SAE approximation.

There is no unique definition of correlation. Here, we associate it with the population exchange between the ground and excited ionic states. In this sense, results for $M = 1$ in Eq. (3) exclude correlation, only exchange is present. Note that Eq. (3) goes beyond the HF ansatz. Indeed, Eq. (6) for $\phi_{j=1}$ includes the coupling to all excited states. Time-dependent HF arises by restricting the sums in Eq. (6) to a single $k = 1$ term, thus losing any coupling between ϕ_1 and other ϕ_k.

Finally, the fc limit is obtained by neglecting the Pauli principle (symmetry) and by dropping the second terms on the left- and the right-hand sides of Eq. (6):

$$i\partial_t \phi_{\mathrm{fc}}(\mathbf{r}_1, t) = \langle \psi_1(\mathbf{r}_2) \mid \mathbf{H} \mid \psi_1(\mathbf{r}_2) \rangle \phi_{\mathrm{fc}}(\mathbf{r}_1, t). \quad (7)$$

The harmonic spectra in the fc approximation, I_{fc} and I^G_{fc}, are calculated using Eqs. (4) and (5) with $\phi_{\mathrm{fc}}(\mathbf{r}_1, t)$, instead of Ψ_M and $\langle \phi_{\mathrm{fc}}(0) | \phi_{\mathrm{fc}}(t) \rangle \phi_{\mathrm{fc}}(0)$ instead of $\alpha(t)\Psi_g$. The prefactor 4 in Eqs. (4) and (5) must be omitted.

Figure 1 shows the harmonic spectrum (a),(b), the ratio of the fc harmonic yield I_{fc} to the full harmonic yield I (c), (d), and I_M/I for $M = 1$, 2, 4 (e,f). The molecular axis is aligned along the laser electric field, i.e., $\theta = 0°$. The left and right panel show the results for Eqs. (4) and (5), respectively. A notable qualitative difference between the two spectra (a),(b) occurs for the harmonics between 19 and 23. The suppression in this range in Fig. 1(b) is due to the two-center interference [14]. In Fig. 1(a) the two-center interference is masked by the polarization of the neutral ignored in Eq. (5). The difference of up to a factor of 30 between (a) and (b) shows the importance of the laser induced polarization of the neutral in HHG.

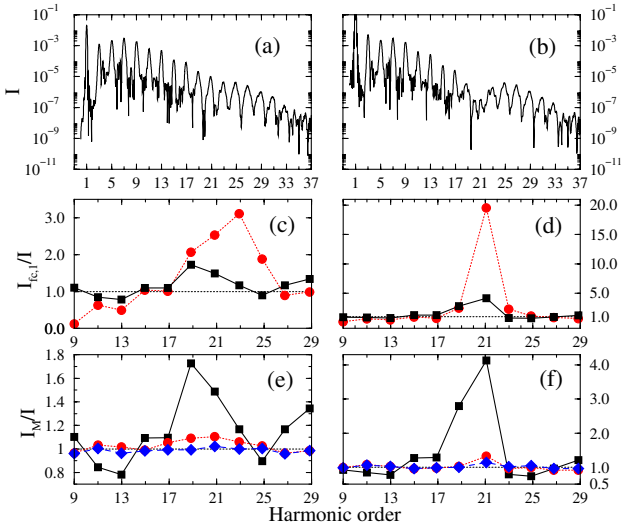

FIG. 1 (color online). Converged full harmonic yields, I and I^G, calculated by (a) Eq. (4), (b) Eq. (5); ratio of frozen core to full harmonic yields, (c) I_{fc}/I and (d) I^G_{fc}/I^G (circles); ratio of IER to full harmonic yields, I_1/I (squares); in the fc calculation I_p was adjusted to match the exact I_p; (e) I_M/I and (f) I^G_M/I^G, for $M = 1$ (squares), $M = 2$ (circles) and $M = 4$ (diamonds). The molecule is aligned along the field, $\theta = 0°$. M is the total number of ionic states included in the IER expansion (3). From fc to $M = 1$ mainly exchange is added. Correlation is systematically built in with increasing M.

For the fc calculation, I_p has been adjusted to that of the two-electron system by adjusting the soft-core parameters of the Coulomb potentials. Nevertheless, the difference from the full result is substantial. Close to the two-center interference minimum, the difference is more than a factor of 3, 20 in Figs. 1(c) and 1(d), respectively.

The result is substantially improved for the eigenstate-resolved approach with $M = 1$, mainly due to accounting for the exchange. The maximum difference to the full result is 1.8 and 4.2 in the range of the two-center interference minimum; see the squares in Figs. 1(e) and 1(f), respectively. Similar to the fc limit, the agreement is improved for the rest of the spectrum, with a difference between 20% and 40%. The expansion converges quickly with increasing M. In I_2 (circles), HHG from the first ionic excited state is added, which improves agreement to within 10% of the full result. The contribution of ψ_3 is negligible due to symmetry. Adding ψ_4 (diamonds) yields almost the full result.

We have also calculated I_1/I and I^G_1/I^G as a function of the alignment angle θ. The maximum difference to the full result is near the two-center interference minimum, which moves to higher harmonics with increasing θ [14].

Thus, the fc model gives a very coarse approximation to HHG. The ionic state expansion allows us to analyze the key missing components. Starting with the fc limit, first the exchange is added for $M = 1$. Correlation is built in with increasing M. For our system, the accuracy of the ground state channel ($M = 1$) is sufficient for many purposes: the contribution of ionic excited states is suppressed by the large energy gap with the ionic ground state. However, for applications such as HHG-based molecular tomography, which relies on the series of harmonic spectra as a function of θ, an error of about a factor of 2–4 in the region of the two-center interference is significant. This error comes from the part of the correlation ($M \geq 2$) that cannot be captured by a SAE analysis. In larger systems, where correlation and polarizability are usually more pronounced, more significant differences are expected. As a result, understanding of the physical origin of the ionic excited state channels is imperative.

Population of the ionic excited states can be caused by the two mechanisms: (i) laser excitation of the two-electron excited states and subsequent decay to ionic excited states during ionization; (ii) virtual and/or real excitations in the ion after ionization, either by the laser field and/or by the recolliding electron.

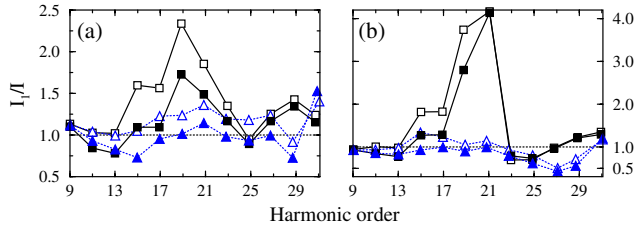

FIG. 2 (color online). I_1/I (a) and I_1^G/I^G (b), determined by replacing the field-free ionic ground state ψ_1 in Eq. (3) with the adiabatic laser polarized ionic ground state $\psi_1(E(t))$ (empty squares); as a reference, I_1/I, I_1^G/I^G from Figs. 1(e) and 1(f) for the field free ionic ground state is plotted (full squares). The results with corresponding empty and full triangles refer to $\theta = 30°$.

The importance of (i) was assessed by projecting the full time-dependent wave function on the two-electron eigenstates (determined by diagonalizing the field-free Hamiltonian). Although two-electron excited states are populated substantially en route to ionization, upon ionization they decay into the ground ionic state. We verified it by repeating the calculation for the above parameters, with the individual excited states as initial state. No substantial population of the ionic excited states was found, ruling out the mechanism (i) for our system.

Regarding the mechanism (ii), excitations by the laser field can be separated into adiabatic polarization (virtual) and nonadiabatic (real) excitations. Nonadiabatic excitations occur when energies of the polarized states change too fast for the electron to follow. Direct simulations of this dynamics between the ground and the first excited state of the ion yields the nonadiabatic excitation probability $P_1^+ \approx 9 \times 10^{-5}$. Hence, the nonadiabatic effects are negligible.

To gauge the effect of the adiabatic polarization, we have replaced the field-free ground state ψ_1 in the wave function (3) with the polarized one, $\psi_1(E(t))$, and calculated I_1/I; see Fig. 2. While the adiabatic polarization is important, it does not generally improve the agreement with the full result and is not the dominant effect.

Thus, the differences between the laser dressed I_1 and I spectra in Fig. 2 are due to the real and virtual excitations of the ion by the recolliding electron. Only in this case the harmonic cutoff is unshifted, in agreement with our simulations. The importance of recollision in our model system was further corroborated by calculating the final population of the ionic states after the laser pulse as a function of the laser polarization. The population of the first excited ionic state is a few percent of the ionic ground state population for linear polarization, and drops to zero with increasing ellipticity.

Our analysis quantifies the importance of various multielectron effects. The difference between I and I^G in Figs. 1(a) and 1(b) shows that neglecting the polarizability of the neutral system can yield order of magnitude differences (see also [18]). To determine the influence of other effects, we use Eq. (5), which excludes the neutral ground state polarization. The difference between I_{fc}^G and I_1^G of up to a factor of 5 is mainly due to exchange. The difference between I_1^G and I^G of more than factor of 4 is due to correlation, major part of which comes from the polarization of the ionic ground state by the returning electron. While the importance of collisional excitations in double ionization has been understood for over a decade, it has been ignored so far in HHG. We expect our conclusions to hold in 3D, since the dimensionality scaling of the recombination and collisional excitation probabilities during the recollision is the same.

All of the multielectron effects identified here will become even more pronounced in extended molecules having higher polarizabilities. This presents a serious challenge for attosecond dynamic imaging of wave functions by molecular tomography. Novel theoretical retrieval tools that can account for multielectron effects are required. One potential path is revealed by our analysis. The fact that only two ionic states in Eq. (6) are important in the HHG in our system shows that one can account for essential multielectron effects by solving several coupled one-electron Schrödinger equations for essential ionic states, leading to dramatic improvement in computational cost.

We acknowledge the support of the NSERC SRO program, Olga Smirnova for fruitful discussions, and Vitali Averbukh for valuable comments.

*s.sukiasyan@uottawa.ca

[1] P. Agostini and L. F. DiMauro, Rep. Prog. Phys. **67**, 813 (2004).
[2] P. Corkum and F. Krausz, Nature Phys. **3**, 381 (2007).
[3] J. Itatani *et al.*, Nature (London) **432**, 867 (2004).
[4] S. Baker *et al.*, Science **312**, 424 (2006).
[5] N. Wagner *et al.*, Proc. Natl. Acad. Sci. U.S.A. **103**, 13 279 (2006).
[6] P. B. Corkum, Phys. Rev. Lett. **71**, 1994 (1993).
[7] S. Patchkovskii *et al.*, Phys. Rev. Lett. **97**, 123003 (2006).
[8] R. Santra and A. Gordon, Phys. Rev. Lett. **96**, 073906 (2006).
[9] Z. Zhao, J. Yuan, and T. Brabec, Phys. Rev. A **76**, 031404 (2007).
[10] A. Gordon *et al.*, Phys. Rev. Lett. **96**, 223902 (2006).
[11] M. Plummer and C. J. Noble, J. Phys. B **35**, L51 (2002).
[12] K. Harumiya *et al.*, Phys. Rev. A **66**, 043403 (2002).
[13] J. S. Parker *et al.*, J. Phys. B **33**, L239 (2000).
[14] M. Lein *et al.*, Phys. Rev. Lett. **88**, 183903 (2002).
[15] K. C. Kulander and B. W. Shore, Phys. Rev. Lett. **62**, 524 (1989).
[16] X. Chu and Shih-I Chu, Phys. Rev. A **64**, 063404 (2001).
[17] M. H. Beck *et al.*, Phys. Rep. **324**, 1 (2000).
[18] G. Jordan and A. Scrinzi, New J. Phys. **10**, 025035 (2008).
[19] J. Zanghellini *et al.*, J. Phys. B **37**, 763 (2004).